Adsorption of Pb(II) ions from contaminated water by 1, 2, 3, 4-butanetetracarboxylic acid-modified microcrystalline cellulose: isotherms, kinetics, and thermodynamic studies

A. Hashem[a], A. J. Fletcher[b], H. Younis[c], H. Mauof[c] and A. Okeil[a]

[a] National Research Center, Textile Research Division, Dokki, Cairo, Egypt.

[b] Department of Chemical and Process Engineering, University of Strathclyde, 75 Montrose Street, Glasgow, G1 1XJ, UK.

[c] Chemistry Department, Faculty of Science, Sebha University., Sebha, Libya.

*Author to whom all correspondence should be addressed. E-mail: alihashem2000@yahoo.com.

Abstract

Microcrystalline cellulose (MCC) has been utilized as an adsorbent material for the removal of Pb(II) ions from aqueous solution after treatment with 1,2,3,4-butanetetracarboxylic acid (BTCA) at elevated temperature to obtain MMCC. The resulting adsorbent was characterized for point of zero point charge (pHZPC), estimation of carboxyl content, fourier transform infrared spectroscopy (FT-IR), scan electron microscopy (SEM), and textural properties, including surface area, and subsequently utilized for the removal of Pb(II) ions from aqueous solution. The adsorption process was probed by investigating the effect of adsorbent dose, pH of solution, temperature, agitation time, and Pb(II) ion concentration. The results showed successful functionalization of MCC using BTCA, which significantly improved the binding properties of the adsorbent towards Pb(II) ions. Isothermal adsorption data was analyzed using Langmuir, Freundlich and Temkin models, evaluated via nonlinear regression analysis. The maximum adsorption

This is a peer reviewed, accepted author manuscript of the following research article: Hashem, A., Fletcher, A. J., Younis, H., Mauof, H., & Abou-Okeil, A. (2020). Adsorption of Pb(II) ions from contaminated water by 1, 2, 3, 4-butanetetracarboxylic acid-modified microcrystalline cellulose: isotherms, kinetics, and thermodynamic studies. International Journal of Biological Macromolecules, 164, 3193-3203. https://doi.org/10.1016/j.ijbiomac.2020.08.159

capacity was found to be 1155 mg/g (at pH 5 and 30 °C) from Langmuir theory, and appears independent of surface area. The Freundlich model was found to provide the best fit and the constant n was determined to be 2.69, indicating that adsorption of Pb(II) ions onto MMCC is favorable. Kinetic modelling showed good agreement for the pseudo-second order kinetic model, supporting the theory that chemisorption is involved in the adsorption process, which is promoted by a high density of active sites. Thermodynamic analysis showed that the adsorption of Pb(II) ions onto MMCC was endothermic and nonspontaneous; hence, MMCC offers an effective method of Pb(II) ion removal from aqueous solutions, with potential for water remediation processes.

Keywords: Microcrystalline cellulose; Isotherm models; Kinetic models.

1. Introduction

Water is a vital component in the survival of living organisms; however, increasing modernization and industrialization is adversely affecting clean water supplies. Species contributing to the pollution of water bodies include heavy metals, dyes, chlorophenols, surfactants, pesticides, herbicides, pharmaceuticals, and personal care products, resulting in negative impacts for both humans and animals through consumption. Due to their inherent toxicity and tendency to bioaccumulate, heavy metals pose a significant risk to human beings and aquatic life [1]. Within this group, lead can enter waterways from storage battery manufacturing processes, lead smelting and refining, and from mining processes. Aqueous phase lead continues to accumulate across the food chain via aquatic species, and by direct absorption [2]. Notable health impacts from Pb(II) poisoning include damage to the nervous system, renal failure, physical weakness, headaches, and brain damage [3], and the maximum concentration of Pb(II) permitted is 0.15 and 0.05 mg /l in drinking and wastewater, respectively [3].

To reduce water contamination, various treatment methods such as neutralization, ion exchange, , solvent extraction, photochemical degradation, electrochemical degradation, membrane separation, reverse osmosis, precipitation and adsorption [4–10] have been investigated for the removal of heavy metals from aqueous streams. From these, one of the most effective methods is adsorption [11], where enhanced surface area, microporous structure, and high degrees of surface reactivity of adsorbents can improve adsorption capacity. Activated carbon offers such parameters as an adsorbent, and is consequently one of the most utilized materials in adsorption processes. Commercial materials can be expensive [12], which drives research to find cheaper, alternative heavy metal adsorbent materials.

Recent studies have focused on creating green adsorbents, often based on cellulose as a consequence of their beneficial physical properties and renewable nature [14]. One family of promising adsorbents that have recently been developed are derived from microcrystalline cellulose (MCC), which offer advantages through use of renewable feedstock, low levels of toxicity, low density, crystallinity, high surface area,

good mechanical strength, insolubility in water and an ability to biodegrade [13]. One drawback to utilizing such materials is that cellulose lacks surface chemical moieties, which are required to complex with targeted heavy metal species. To counter this, esterification [15], etherification [16], oxidation [17], and graft copolymerization [18] have been used to functionalize cellulose to make it a stronger and more effective adsorbent.

The aim of the present work was to develop a cellulose-based bioadsorbent for the extraction of Pb(II) ions from aqueous solutions using batch adsorption techniques, by modifying microcrystalline cellulose using butanetetracarboxylic acid. The effect of adsorption reaction conditions, including pH, adsorbent dosage, adsorbate concentration , contact time and temperature, on the adsorption capacity of Pb(II) ions were examined. The most suitable adsorption and kinetic models for the adsorption of Pb(II) onto modified MCC were determined by nonlinear regression methods. Thermodynamic parameter for this system was also determined.

2. Materials and Methods

2.1. Materials

Microcrystalline cellulose (MCC), ~50 µm particle size, 1, 2, 3, 4-butanetetracarboxylic acid (BTCA), lead acetate, ethylenediaminetetraacetic acid (EDTA), nitric acid (HNO_3), sodium hydroxide (NaOH) and ethanol were supplied from Merck (Germany) and used as received (laboratory grade).

2.2. Methods

2.2.1. Adsorbate

A stock solution of Pb2+ was prepared (1000 mg/l) by dissolving the required amount of, Pb(CH3.COO)2 in double distilled water. The stock solution was diluted with double distilled water to obtain desired concentration, ranging from 100 to 1000 mg/l.

2.2.2. Preparation of the adsorbent

The modified microcrystalline cellulose (MCCC) adsorbent was prepared in a beaker containing 2 g of microcrystalline cellulose (MCC) powder and a known weight of a dissolved 1, 2, 3, 4-butanetetracarboxylic acid (BTCA) in water and stirred with a spatula. The homogeneous paste was then dried in an oven at 100–160 °C and subsequently cooled to room temperature. The sample was washed with ethanol/water (80:20) for 2 h using vacuum suction filtration to remove any unreacted BTCA and soluble by-products. The purified material was dried at 80 °C for 3 h.

Using a high temperature for a synthetic procedure involving BTCA, results in the anhydride form of the chemical to be produced, which reacts with the hydroxyl groups of MCC during heating to form the final MMCC adsorbent, as shown in Scheme 1:

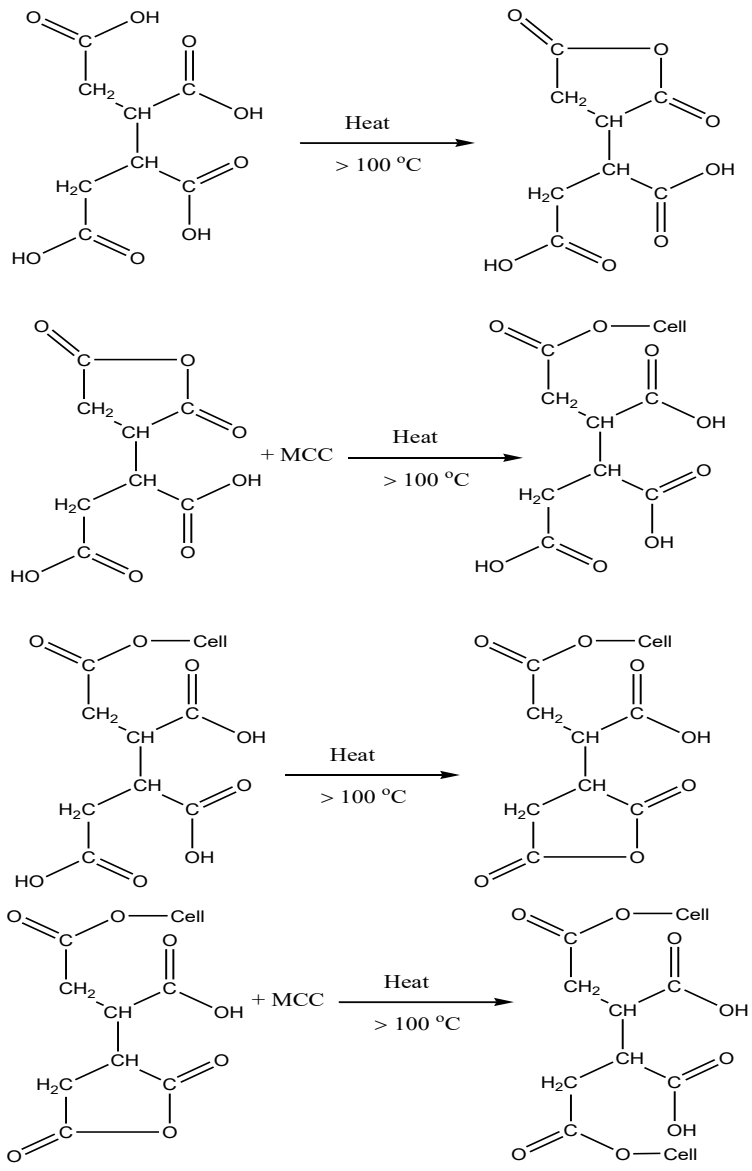

Scheme1: Reaction of MCC with BTCA to form MMCC at high temperature.

2.2.3. Batch Adsorption Studies

A weighed sample of adsorbent (0.03 g) was added to a known volume (100 mL) of a Pb(II) ion solution (100–1000 mg L^{-1}) in a 125 mL Erlenmeyer flask. 0.1 M HNO_3 or 0.1 M NaOH was added to adjust initial pH values. The mixture was shaken at a constant speed of 150 rpm at 30 °C for a defined period of time and filtered using Whatman No. 41 filter paper to separate the adsorbent and metal ion solution. The

metal ion concentration was measured before and after the adsorption using direct titration with a standard EDTA solution.

The amount of Pb(II) adsorbed at equilibrium, q_e (mg/g) was calculated using Equation (1):

$$q_e = \frac{(C_o - C_e).V(l)}{W} \quad (1)$$

The percentage removal was calculated according to Equation (2):

$$\text{Removal}\% = \frac{C_o - C_e}{C_o} \cdot 100\% \quad (2)$$

where C_o and C_e (mg L^{-1}) are the initial metal concentration and metal concentration at equilibrium, W (g) is the weight of the adsorbent and V (L) is the volume of Pb(II) solution.

2.2.4. Effect of temperature experiment

The effect of temperature is crucial in determining the effective working capacity of a material under given operating conditions, consequently, the adsorption capacity of Pb(II) ions onto MMCC was determined at pH 5.5, for an adsorbent dose of 0.3 g L^{-1}, at 30, 50, and 60 °C.

2.2.5. Carboxyl content

Carboxyl group contents of the adsorbent samples were estimated by adding 0.2 g of the adsorbent to a 125 mL flask containing 50 mL NaOH solution (0.03 N). The flasks were left overnight to equilibrate at room temperature and then the carboxyl contents determined via titration with standard HCl solution (0.01 N) using a phenolphthalein indicator [19]. The carboxyl content of the adsorbent sample was calculated using Equation (3):

$$[COOH]m.eq/100g\ sample = \frac{(V_0 - V_l) \cdot N \cdot 100}{wt} \quad (3)$$

where V_o is the HCl volume (mL) consumed without the addition of the adsorbent in the blank experiment, V_l is the HCl volume (mL) consumed by the adsorbent sample, N is the normality of the standard HCl solution, and W is the weight of the adsorbent sample (g).

2.2.6. Characterization of the adsorbent

Fourier transform infrared spectroscopy

Samples of MCC, MMCC, and MMCC loaded with Pb(II) post-adsorption were characterized using Fourier Transform infrared spectroscopy (FTIR) to assign vibrational frequencies of the different functional groups present in the parent adsorbent structure, as well as to determine the nature of any bonds formed between Pb(II) ions and the adsorbent surface. FTIR spectra of KBr discs containing ~2-10 mg of sample in ~300 mg of KBr were recorded using a Perkin–Elmer Spectrum1000 spectrophotometer over a wavelength range of 4000–400 cm^{-1} at a scan interval of 1 cm^{-1} over 120 scans.

Scanning electron microscopy (SEM)

A sample of each sorbent was coated with chromium on carbon tape and then imaged using a TESCAN CE VEGA 3 SBU (117-0195- Czech Republic) scanning electron microscope (SEM). Images were recorded using 1000 x magnification and the technique provided information on the morphology of the parent MCC and the MMCC adsorbent.

Energy–dispersive X-ray analysis (EDX)

Energy-dispersive X-ray (EDX) patterns were recorded using a dispersive X-ray fluorescence (EDX) spectrometer (Oxford Instruments) attached to a scanning electron microscope (JEOL-JSM-5600). The characteristic band of lead metal was used to confirm the presence or absence of Pb(II) ions on post-adsorption MMCC samples.

BET surface area measurement

The textural characteristics of MMCC were determined via nitrogen adsorption using an Autosorb I assembly (Nova 2000, Quantahrome Instrument, Beach, USA). Analysis was conducted using oxygen-free nitrogen gas at-196 °C, and the isothermal data obtained analyzed using the Brunauer-Emmet-Teller (BET) method [20]. Mesopore volume, external surface area, and mesopore surface area were determined using the t-plot method [21,22], while the Barrett-Joyner-Halenda technique [23] was used to calculate the average pore width and obtain the pore size distribution.

Determination of point of zero charge (pH_{pzc})

A solid addition method was used to evaluate the pH at the point of zero charge pH_{pzc} for MMCC. Typically, 100 mL of 0.01 N NaCl was added to a series of conical flasks and the pH adjusted using an aqueous solution of 0.01 N HCl and 0.01 N NaOH to adjust the pH within the range 2 to12. The initial pH was recorded after a constant pH value was attained; thereafter,~100 mg of the adsorbent was dispersed in the conical flasks and incubated for 24 h to obtain the final pH. The initial and final pH was plotted, with the point of intersection of the plots denoting the pH_{pzc} of the adsorbent.

2.3. Error analysis

Models used to fit the isothermal data obtained in this study were optimized by defining an error function to evaluate the fit of the isotherm to the experimental equilibrium data. The error selected were average relative error (ARE), average percentage error (APE %), sum squares error (ERRSQ/SSE), hybrid fractional error function (HYBRID), Marquardt's percent standard deviation MPSD, sum of absolute error (EABS), nonlinear chi-square test (χ^2), and coefficient of determination (R^2) [24-31], as shown in Table 1.

3. Results and Discussion

3.1. Adsorbent characterization

In order to confirm the modification of MCC by BTCA, the surface functional properties of MCC, MMCC and MMCC-loaded Pb(II) were investigated. The spectra of native MCC (Figure 1a), exhibited adsorption bands at 3326 cm^{-1} (due to stretching frequency of the -OH group), 2892 cm^{-1} (due to C-H stretching vibration), 1644 cm^{-1} (due to bound water absorption [32,33]), and 1429 cm^{-1} (due to -CH_2 scissoring). The absorption band at ~1023 cm^{-1} was ascribed to C-O stretching vibrations, which symbolizes the glucose ring, and the intensity of this peak was unchanged after modification. Figure 1b shows that additional peaks were observed for MMCC; 1715 cm^{-1} is assigned to the stretching vibration of the newly formed ester carbonyl groups from modification of MCC with BTCA, while the characteristic peak located in 1428 cm^{-1} is ascribed to the -OH bending vibration from -COOH. This demonstrates the successful modification of MCC with BTCA. Figure 1(c) shows a small decrease in the absorbance peaks obtained for Pb(II)-loaded MMCC, as compared with that in MCC and MMCC, the bands previously observed at 3329, 1717 and 1645 cm^{-1} were shifted to 3328, 1714 and 1643 cm^{-1}, respectively, while new peaks are observed at 2094 and 1025 cm^{-1}, which can be attributed to the adsorption of Pb(II)ions onto MMCC.

The surface morphology of MMCC is presented in Figure 2a, and reveals a cluttered and agglomerated material with few pores. It should be noted that there are no critical changes in surface morphology after adsorption of Pb(II) ions (Figure 2b), except some sort of swellability potentially through diffusion of Pb(II) ions inside the fine structure of MMCC, indicating that MMCC is a robust adsorbent with favorable potential for commercialization. The EDX spectra of Pb(II)-loaded MMCC is presented in Figure 2c. The presence of sharp peaks corresponding to elemental Pb in the Pb(II)-loaded MMCC sample confirms the adsorption of Pb(II) onto the MMCC surface.

The textural characteristics of MCC show a BET surface area of 2.9 $m^2\ g^{-1}$ with a total pore volume of 0.004 $cm^3\ g^{-1}$, and an average pore width of 5 nm, and the average surface area is unaffected by conversion to MMCC. The average pore width is in the macropore region [34], which is beneficial for mass transport, particularly in aqueous systems, enhancing the adsorption of Pb(II) ions.

3.2. Factors affecting preparation of MCC treated with BTCA

Effect of BTCA concentration

Figure 3a shows the dependence of BTCA concentration on the extent of modification of MCC, expressed as m.eq.-COOH/100g sample. As expected, the carboxyl content increases significantly from 133.3 to 230.5 m.eq./100 g sample with increasing BTCA concentration, from 2.14 to 8.55 mmol/L; higher concentrations resulted in a plateaued maximum level of functionalization. This behavior can be ascribed to the increasing availability of BTCA molecules in close proximity with MCC macromolecules, as shown previously in Scheme 1, BTCA is converted to the corresponding anhydride through dehydration under the effect of high temperature before subsequent reaction with the hydroxyl groups in the MCC cellulose structure.

The hydroxyl groups in the cellulose molecule are essentially the functional sites at which the esterification reaction occurs. Since these groups are immobile, it is essential that there should be a greater availability of butanetetracarboxylic acid molecules in the vicinity of the cellulose hydroxyl groups if reaction is to occur.

Effect of reaction temperature

The effect of reaction temperature on the extent of modification when MCC particles were treated with BTCA at different temperatures is shown in Figure 3b. The carboxyl content of MCC treated with BTCA increases from 52 to 230.5 m.eq/100g sample when increasing the reaction temperature from 100 to 140 °C; a decrease in carboxyl content is observed for reaction temperatures greater than 140 °C. The enhancement in carboxyl content of MMCC for temperatures in the range 100-140 °C may be associated with favorable thermal effects on cellulosic swelling and accessibility for reaction, the conversion of BTCA to its anhydride analogue, as well as increased mobility and reactivity of the resulting BTCA anhydride molecules with MCC to form MMCC. At higher temperatures, catalytic effects may hinder successful

reaction and temperatures in excess of 160 °C were not used due to the conversion of cellulosic material to ash at such temperatures.

Effect of dehydration time

MCC was modified through treatment with BTCA at a fixed temperature of 140 °C but using different reaction times of 15-180 min. It is evident from Figure 3c that the carboxyl group content of MMCC increased significantly from 128 to 232 m.eq/100 g sample for reaction times increasing from 15 to 60 min, before a subsequent decrease at longer reaction times. As may be expected, increased contact time can be seen to increase the level of functionalization, as seen here for MMCC, however, the decrease in carboxyl content from 210 to 143 m.eq/100g sample, observed for an increase from 60 to 180 min reaction time [35].

3.3. Factors affecting the adsorption of Pb(II) onto MMCC

Point of Zero Charge (pH_{pzc}) and the effect of pH Data obtained for adsorption of Pb(II) ions by MMCC at pH range 2.0–5.0, and an initial Pb ion concentration of 400 mg/L, is shown in Figure 4a and allows the effect of pH to be probed. The adsorption of Pb(II) ions increased from 57 to 667 mg/g by increasing pH from 3.0 to 5.0. Within the system studied, there are two main steps that occur according to Equations 4 and 5 as follows:

$$2MMCC-COOH \Leftrightarrow 2MMCC-COO^{-}+2H^{+} \quad (4)$$

$$2MMCC-COO^{-}+Pb^{2+} \Leftrightarrow (MMCC-COO)_2 \cdot Pb \quad (5)$$

Equation 4 represents deprotonation, the first stage in ion exchange, while equation 5 represents the adsorption of Pb(II) ions onto the deprotonated MMCC. The adsorption capacity, q_e, of Pb(II) at pH 2 is zero, this can be ascribed to high concentration of the H^+ in solution at highly acidic pH, which shifts the equilibrium in Equation 4 mainly to the left, hence the active -COOH groups are not ionized and the ion exchange sites on the MMCC surface are still protonated. Under these solution conditions, the bulk of the

metal ion remains in solution. As the pH increases from 3 to 5, the adsorption capacity of Pb(II) increases as the equilibrium in Equation 4 shifts to the right, ionizing the carboxyl groups, and providing sites for interaction of the Pb(II) ions.

Figure 4b shows the pH_{pzc} data obtained for the surface of the MMCC adsorbent. The pH_{pzc} of MMCC was determined as 4.0, which denotes the point at which a neutral charge is obtained and indicating an acidic nature for the surface of the MMCC adsorbent. When the solution pH is higher than the pH_{pzc}, the surface will be predominately negatively charged and likewise will be predominately positively charged if the solution pH is lower than pH_{pzc} [36], and the pH_{pzc} can consequently provide insight into the electrostatic interactions between the surface of the adsorbent and adsorbate [37]. When the pH value of the solution is higher than pH_{pzc}, the charge of MMCC surface will be negative and binding of cations will be favored. When the pH value of the solution is lower than the pH_{pzc}, the surface charge of an adsorbent will be positive and, therefore, the adsorption of cations is unfavorable [38]. The optimum pH for MMCC to adsorb Pb(II) is 5.0 (Figure 4a) which is higher than the $pH_{pzc.}$ This leads to the predominant negativity of the adsorbent surface, which may lead to electrostatic attraction between the Pb(II) ions and negatively charged surface [39].

Effect of adsorbent concentration The mass of adsorbent available within the system influences the adsorption of metal uptake from solution. The effect of MMCC adsorbent amount on adsorption capacity was studied at pH 5 using adsorbent doses in the range of 0.3–10 g/L and at an initial metal ion concentration of 400 mg/L (Figure 5a). It is evident that the adsorption capacity (q_e) of Pb(II) ions per unit mass of adsorbent decreased from 664 to 37 mg/g, as adsorbent dose increased from 0. 3 to 8 g/L, with a plateau observed at higher adsorbent dosing. The decrease in adsorption capacity with increasing adsorbent dose is attributed to the high number of unsaturated adsorption sites, as well as overlap of adsorption sites and overcrowding of adsorbent particles [40].

Effect of contact time and adsorbate concentration The effect of contact time on the adsorption capacity of MMCC towards Pb(II) ions, at initial adsorbate concentrations of 303 and 493 mg/L, is shown in Figure 5b. The adsorption capacity is seen to increase with both increasing contact time and increasing initial adsorbate concentration of the adsorbate. Equilibrium was determined to have been achieved at 120 min above which a plateau is observed.

3.4. Isotherm modelling

The Langmuir equation [41] is based on monolayer adsorption for a fixed number of localized sites, with homogeneous adsorption and no movement of adsorbate in the surface plane. The non-linear form of the Langmuir isotherm is represented by Equation (6):

$$q_e = \frac{k_L.C_e}{1 + a_L.C_e} \tag{6}$$

where K_L refers to the Langmuir constant (L/g), a_L is the Langmuir isotherm constant (L/mg), and k_L/a_L is the maximum adsorption capacity (q_{max}). The dimensionless separation factor, R_L, provides an indication of the favorability of the adsorption process [42], and is represented by Equation (7):

$$R_L = \frac{1}{(1 + b.C_0)} \tag{7}$$

where C_o is the initial adsorbate concentration in solution and b is the Langmuir constant.

The logarithmic form of Freundlich model is expressed by equation 8 [43]:

$$q_e = K_F.C_e^{1/n} \tag{8}$$

Where C_e is the concentration of Pb(II) ions at equilibrium, mg/L, q_e is the amount of adsorbed Pb(II) ions per unit of weight (mg/g), and K_F and n are Freundlich constants related to the adsorption capacity and favorability, respectively.

The non-linear form of the Temkin isotherm [44] is represented by Equation (9):

$$q_e = \frac{RT}{b_T} \ln(A_T C_e) \quad (9)$$

where A_T is the Temkin isotherm constant (l/g), b_T is the Temkin constant of heat of adsorption (joules/mole), T is the absolute temperature, and R (8.314 J/mol K) is the gas constant.

Error analysis

Minimization of the error distribution between the experimental data and the data derived from predicted isotherms was performed using non-Linear analysis of a series of error functions. Experimental data were analyzed using the aforementioned two-parameter isotherm models, which were optimized using analysis of the average relative error (are), average percentage error (APE %), sum squares error (ERRSQ/SSE), sum of absolute error (EABS), and the coefficient of determination (R^2). Figure 5c shows the comparison between experimental and theoretical data of the two parameter isotherm models used in this study,

Table 2 shows that the MMCC produced within the present work has a high affinity for the removal of Pb(II) ions (1155 mg/g) from solution when compared with modified Ratama raetam (270.27 mg/g) and other various adsorbents previously reported in the literature [45-51].

The resulting error analysis and constants of the isotherm models are provided in Table3. As stated above R_L from the Langmuir model indicates the favorability of the adsorption process; the value obtained here was 0.578, indicating favorable adsorption (irreversible (R_L=0), linear (R_L=1), favorable (0<R_L<1), or unfavorable (R_L>1)). Additionally, the value of n, as determined from the Freundlich model (Table 3) was 2.69, again indicating that the adsorption of Pb(II) ions onto MMCC is favorable; however, a value of 1/n < 1 suggests a slight suppression of adsorption at lower equilibrium concentrations. The maximum adsorption capacity of Pb(II) ions onto MMCC, according to Langmuir analysis was 1155 mg/L, which represents a significant level of available adsorption potential. Overall, as see in Figure 5c and Table 3, the

highest R^2 value and lowest ARE, APE %, EABS and ERRSQ values indicate that the Freundlich model provides the best fit to the experimental isotherm data obtained in this study.

3.5. Adsorption kinetics

The equilibrium capacity of an adsorption system must be matched by suitable kinetic performance for potential application of such adsorbents. In the present study four models were used to analyze the kinetics of adsorption for Pb(II) ions on MMCC, namely pseudo-first-order, pseudo second-order, Bangham, and intra-particle diffusion models. As for the adsorption models discussed above, the same series of fitting functions were used to determine the quality of the fits between experimental theoretical data.

The pseudo-first order model is based on a physical and diffusion controlled process; the non-linear form of the model [52] is given in Equation 10:

$$q_t = q_e[1 - \exp(-k_1 t)] \quad (10)$$

where q_t is the amount of Pb(II) ions adsorbed (mg.g^{-1}) at time t (min), q_e is the amount of Pb(II) ions adsorbed (mg.g^{-1}) at equilibrium and k_1 is the rate constant (min^{-1}).

The pseudo-second order kinetic model [53] is assumed to involve physicochemical interactions between the adsorbent and adsorbate; the non-linear form of the model given in Equation 11:

$$q_t = k_2 . q_e^2 . t / (1 + k_2 . q_e . t) \quad (11)$$

Where q_t, q_e and t are as defined above, and k_2 (g.mg^{-1} min^{-1}) is the rate constant for the kinetic model.

Diffusion mechanisms cannot be elucidated by either the pseudo-first-order or pseudo-second-order kinetic models, hence, the intra-particle diffusion model is also used to evaluate the kinetic results. The overall kinetics of adsorption when controlled by intra-particle diffusion [54] can be expressed by Equation 12:

$$q_t = k_{id}.t^{0.5} + C \quad (12)$$

where q_t and t are as defined above, k_{id} ($mg.g^{-1}min^{1/2}$) is the intra-particle diffusion rate constant, C ($mg.g^{-1}$) is the concentration of Pb(II) at equilibrium. Previous studies reported that that the plots of q_t vs. $t^{1/2}$ are multi-linear steps controlled the adsorption process [55, 56]. Initially a curve is observed, indicative of bulk diffusion, followed by a linear portion, attributed to intra-particle diffusion, and finally a plateau once equilibrium is achieved.

Bangham's kinetic model can be used to determine whether pore diffusion is the only rate-controlling step [57], through the quality of the fit, and is expressed by Equation 13:

$$q_t = q_e[1 - \exp(-k_b.t^n] \quad (13)$$

where q_t, q_e and t are as defined above, and k_b is the rate constant for the model.

In all cases, Table 4 shows the parameters determined for each model and the fitting parameters for the selected error functions. From fits shown in Figure 6 (a, b, c and d) and the data presented in Table 4, it is evident that the highest correlation function and lowest values for all other error functions, indicate that the Bangham and pseudo second-order kinetic models provide the best fits to the experimental data. This suggests that the adsorption process is controlled by chemisorption [58] and that pore diffusion is the only rate-controlling step in the process.

3.6. Effect of temperature and thermodynamic parameters

The data obtained in Figure 7 indicate that the adsorption capacity increases with increasing temperature. In the present work, thermodynamic parameters, including the standard free energy (ΔG^o), enthalpy change (ΔH^o) and entropy change (ΔS^o) were calculated through the application of Equations 14-16 [59]. The standard free energy (ΔG^o) was calculated from Equation 14:

$$\Delta G° = -RT \ln a_L \quad (14)$$

where a_L is the Langmuir constant, R is the universal gas constant (8.31441 J/mol·K) and T is the absolute temperature (K). The Langmuir constant, a_L, can be used in the van't Hoff equation to determine the enthalpy change, ΔH°, of the adsorption process as a function of temperature (Equation 15) as follows:

$$\ln(\frac{a_{L2}}{a_{L1}}) = \frac{\Delta H^o}{R} . \frac{(T_2 - T_1)}{T_1 . T_2} \quad (15)$$

where a_{L1}, a_{L2} and a_{L3} are the Langmuir constants at 30, 50 and 60 °C, respectively. The positive values of ΔG° obtained using Equation 14 and listed in Table 5 indicate the nonspontaneous nature of the adsorption of Pb(II) ions onto MMCC, which may be related to the chemical interactions of complexation. Additionally, a positive value was obtained for ΔH° in the range of 30–60 °C, using Equation 15 and is shown in Table 5; this suggests that the adsorption process of Pb(II) ions onto MMCC is endothermic over this temperature range, which is indicative of a chemisorption process. Finally, the entropy change (ΔS°) was calculated from Equation 16:

$$\Delta G^o = \Delta H^o - T\Delta S^o \quad (16)$$

and the positive value of ΔS° in the range of 30–60 °C, is related to an increase in randomness at the solid/solution interface during the adsorption of Pb(II) ions onto MMCC. This can be ascribed to the deprotonation of the carboxylic groups and chelation of Pb(II) increasing the disorder within the chemistry of the system.

3.7. Mechanism of adsorption

Understanding the adsorption mechanism of heavy metal onto adsorbent makes it easier to remove heavy metals during wastewater treatment. It Is clear that the removal of Pb(II) ions from aqueous solution onto MMCC may be described by two steps; firstly, deprotonation of the carboxyl groups on the surface of MMCC, which resulted from the thermal treatment of MCC with BTCA, followed by a second

step of chelation (complexation) between the electron-accepting Pb(II) ions and the electron-donating oxygen atoms of the carboxyl groups of MMCC as shown in Scheme 2. Such behavior was also observed for Cd(II) adsorption on modified pine sawdust [40].

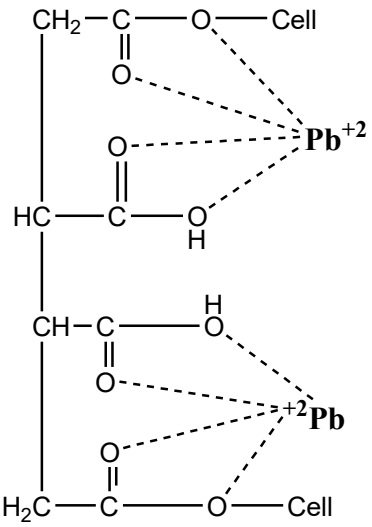

Scheme 2: Complex structure between MMCC and Pb(II) ions.

4. Conclusions

Micocrystalline cellulose was modified by treatment with 1, 2, 3, 4-butanetetracarboxylic acid to obtain modified microcrystalline cellulose (MMCC). The factors affecting the extent of surface modification showed that there were limiting values for reactant concentration, reaction time and reaction temperature. The extent of surface modification was determined by evaluation of the carboxyl content of MMCC adsorbent samples, with optimized samples (231 m.eq/100 g sample) used for removal of Pb(II) ions from aqueous solution by a batch adsorption procedure. The results obtained indicate that the adsorption capacity of MMCC towards Pb(II) ions was affected by initial pH, adsorbent dose, contact time and temperature. Adsorption data obtained under optimized conditions of pH 5, 0.3 g/L of adsorbent, 30 °C for 3h was analyzed using Langmuir, Freundlich and Temkin models, and evaluated using non-linear regression techniques. The results obtained showed that the maximum adsorption capacity according to the Langmuir equation was 1155 mg/g, while the kinetics of adsorption could be described well by

Bangham's model and the pseudo-second-order kinetic model, indicating chemisorption within the adsorption process. Thermodynamic studies indicated that the adsorption process was non-spontaneous and an endothermic reaction with increased disorder in the adsorption system; all of which supports a process of surface group deprotonation and chelation of Pb(II) ions. These adsorbents show excellent performance for heavy metal ion remediation, which may be extend to other metals and inform engineering solutions for water treatment.

References

[1] Z. N. Garba, I. Lawan, W. Zhou, M. Zhang, L. Wang, Z. Yuan, Microcrystalline cellulose (MCC) based materials as emerging adsorbents for the removal of dyes and heavy metals: A review, Science of the Total Environment 717 (2020) 135070.

[2] M. N. Rashed, Lead removal from contaminated water using mineral adsorbents. The Environmentalist 21(2001)187–195.

[3] Poonam, S. K. Bharti, N. Kumar, Kinetic study of lead ($Pb2^{+}$) removal from battery manufacturing wastewater using bagasse biochar as biosorbent, Applied Water Science 8 (2018) 119.

[4] D. Gusain , V. Srivastava, Y.C. Sharma, Kinetic and thermodynamic studies on the removal of Cu (II) ions from aqueous solutions by adsorption on modified sand, J. Ind. Eng. Chem. 20 (3) (2014) 841–847.

[5] T. Falayi, F. Ntuli, Removal of heavy metals and neutralization of acid mine drainage with un activated attapulgite, J. Ind. Eng. Chem. 20 (4) (2014) 1285–1292.

[6] A.Janin, J.F. Blais, G. Mercier, P. Drogui, Selective recovery of Cr and Cu in leachate from chromated copper arsenate treated wood using chelating and acidic ion exchange resins , J. Hazard. Mater. 169 (1–3) (2009) 1099–1105.

[7] S.Y. Bratskaya, A.V. Pestov, Y.G. Yatluk, V.A. Avramenko, Heavy metals removal by flocculation/precipitation using N-(2-carboxyethyl) chitosans, Colloids Surf. A Physicochem. Eng. Asp. 339 (1–3) (2009) 140–144.

[8] T.K. Tran, H. J. Leu, K.F. Chiu, C.Y. Lin, Electrochemical treatment of heavy metal containing wastewater with the removal of COD and heavy metal ions, J. Chin. Chem. Soc. 64 (5) (2017) 493–502.

[9] J. Liu , P. Wu, S. Li, M. Chen, W. Cai, D. Zou, N. Zhu, Z. Dang, Synergistic deep removal of As(III) and Cd(II) by a calcined multifunctional MgZnFe-CO3 layered double hydroxide: Photooxidation, precipitation and adsorption, Chemosphere, 225(2019) 115-125.

[10]L. Chen, P. Wu, M. Chen, X. Lai, Z. Ahmed, N. Zhu, Z. Dang, Y. Bi, T. Liu, Preparation and characterization of the eco-friendly chitosan/vermiculite biocomposite with excellent removal capacity for cadmium and lead, Applied Clay Science 159(2018)74-82.

[11] A. Hashem, A. Al-Anwar, N.M. Nagy, D.M. Hussein, S. Eisa, Isotherms and kinetic studies on adsorption of Hg (II) ions onto Ziziphus spina-christi L. from aqueous solutions, Green Process. Synth. 5 (2016) 213–224.

[12] J.-S. Kwon, S.-T. Yun, J.-H. Lee, S.-O. Kim, H.Y. Jo, Removal of divalent heavy metals (Cd, Cu, Pb, and Zn) and arsenic (III) from aqueous solutions using scoria: kinetics and equilibria of sorption, J. Hazard. Mater. 174 (2010) 307–313.

[13] Z. Dong, L. Zhao, Covalently bonded ionic liquid onto cellulose for fast adsorption and efficient separation of Cr(VI): batch, column and mechanism investigation, Carbohyd. Polym. 189 (2018a) 190–197.

[14] B. Li, Y. Pan, Q. Zhang, Z. Huang, J. Liu, H. Xiao, Porous cellulose beads reconstituted from ionic liquid for adsorption of heavy metal ions from aqueous solutions. Cellulose 26(2019) 9163-9178.

[15] G. Yana , B. Chena , X. Zeng , Y. Sun , X. Tang , L. Lin, Recent advances on sustainable cellulosic materials for pharmaceutical carrier applications: A review, Carbohydrate Polymers, 244(2020) 116492.

[16] A. Hashem, A. M. Azzeer, and A. Ayoub, The Removal of Hg (II) Ions from Laboratory Wastewater onto Phosphorylated Haloxylon ammodendron: Kinetic and Equilibrium Studies, Polymer-Plastics Technology and Engineering 49(2010) 1463–1472.

[17] S.Zaccaron, U. Henniges , A. Potthast, T. Rosenaua, How alkaline solvents in viscosity measurements affect data for oxidatively damaged celluloses, Cuoxam and Cadoxen, Carbohydrate Polymers, 240 (2020) 116251.

[18] D.-F. Hou, , Z.-Y. Liu, L. Zhou, H. Tan, W. Yang, M.-B. Yang, A facile strategy towards heterogeneous preparation of thermoplastic cellulose grafted polyurethane from amorphous regenerated cellulose paste, International Journal of Biological Macromolecules, 161(2020) 177-186.

[19] M.I. Khalil, A. Hashem, A. Hebeish, Carboxymethylation of Maize Starch Starch-Stärke 42 (1990) 60–63.

[20] S. Brunauer, P.H. Emmett, E. Teller, Adsorption of gases in multimolecular layers, Journal of the American chemical society 60 (2) (1938) 309-319.

[21] B. C. Lippens, and J. H. De Boer, Studies on pore systems in catalysts: V. The t method, Journal of Catalysis 4(3) (1965) 319-323.

[22] F. Rouquerol, J. Rouquerol, K. S. W. Sing, Assessment of mesoporosity, Adsorption by Powders and Porous Solids, 2nd Edition, (1999) 191-217.

[23] E.P. Barrett, L.G. Joyner, and P.P. Halenda, The determination of pore volume and area distributions in porous substances. I. Computations from nitrogen isotherms. Journal of the American Chemical society 73 (1) (1951) 373-380.

427 [24] A. Kapoor, , R.T. Yang, Correlation of equilibrium adsorption data of condensable vapours on porous
428 adsorbents, Gas Sep. Purif. 3 (1989) 187–192.

429 [25] S. Rangabhashiyam, N. Anu, M. Nandagopal, Relevance of isotherm models in biosorption of
430 pollutants by agricultural byproducts, J. Env. Chem. Eng. 2(1) (2014) 398-414

431 [26] K.V. Kumar, , S. Sivanesan, Pseudo second order kinetics and pseudo isotherms for malachite green
432 onto activated carbon: comparison of linear and nonlinear regression methods, J. Hazard. Mater. B136
433 (2006) 721–726.

434 [27] J.C.Y. Ng, W.H. Cheung, G. McKay, Equilibrium studies of the sorption of Cu(II) ions onto chitosan, J.
435 Colloid Interface Sci. 255 (2002) 64–74.

436 [28] D.W. Marquardt, An algorithm for least-squares estimation of nonlinear parameters, J. Soc. Ind. Appl.
437 Math. 11 (1963) 431–441.

438 [29] J.C.Y. Ng, W.H. Cheung, G. McKay, Equilibrium studies for the sorption of lead from effluents using
439 chitosan, Chemosphere 52 (2003) 1021–1030.

440 [30] B. Boulinguiez, P. Le Cloirec, D. Wolbert, Revisiting the determination of Langmuir parameters
441 application to tetrahydrothiophene adsorption onto activated carbon, Langmuir 24 (2008) 6420–6424.

442 [31] K. Vijayaraghavan , T.V.N. Padmesh, K.Palanivelu, M. Velan, Biosorption of nickel(II) ions onto
443 Sargassum wightii: application of two-parameter and three-parameter isotherm models. J. Hazard. Mater.
444 133 (2006), 304-308.

445 [32]H. M. Ahsan, X. Zhang, Y. Li, B. Li, S. Liu, Surface modification of microcrystalline cellulose:
446 Physicochemical characterization and applications in the Stabilization of Pickering emulsions,
447 International Journal of Biological Macromolecules 132 (2019) 1176–1184.

448 [33] C. Shi, F. Tao, Y. Cui, Evaluation of nitriloacetic acid modified cellulose film on adsorption of methylene
449 blue, International Journal of Biological Macromolecules 114 (2018) 400–407.

450 [34] I. Khalil, K. Thomas, H. Jabraoui, P. Bazin, F. Maugé, Selective elimination of phenol from hydrocarbons
451 by zeolites and silicabased adsorbents—Impact of the textural and acidic properties, Journal of Hazardous
452 Materials 384(2020)121397.

453 [35] A. Hashem, H. A. Hammad and A. Al-Anwar, Modified Camelorum tree particles as a new adsorbent
454 for adsorption of Hg(II) from aqueous solutions: kinetics, thermodynamics and non-linear isotherms,
455 Desalination and Water Treatment 57(2016):1-17.

456 [36] O. Hamdaoui, Batch study of liquid-phase adsorption of methylene blue using cedar sawdust and
457 crushed brick, J. Hazard. Mater. 135 (2006) 264–273.

458 [37] W.S.W. Ngah, L. C. Teong, R.H. Toh, M.A.K.M. Hanafiah, Utilization of chitosan–zeolite composite
459 in the removal of Cu (II) from aqueous solution: adsorption, desorption and fixed bed column studies,
460 Chem. Eng. J. 209 (2012) 46–53.

461 [38] M. Martín-Lara, F. Hernáinz, M. Calero, G. Blázquez, G. Tenorio, Surface chemistry evaluation of
462 some solid wastes from olive-oil industry used for lead removal from aqueous solutions, Biochem. Eng. J.
463 44 (2009) 151–159.

464 [39] H.Chen, Y. Zhao, A. Wang, Removal of Cu (II) from aqueous solution by adsorption onto acid-
465 activated palygorskite, J. Hazard. Mater. 149 (2007) 346–354.

466 [40] A. Hashem, S.M. Badawy, S. Farag, L.A. Mohamed, A.J. Fletcher, G.M. Taha, Non-linear adsorption
467 characteristics of modified pine wood sawdust optimised for adsorption of Cd(II) from aqueous systems,
468 Journal of Environmental Chemical Engineering for adsorption of Cd(II) from aqueous systems,
469 8(2020)103966.

[41] I. Langmuir, The constitution and fundamental properties of solids and liquids. Part I. solids, J. Am. Chem. Soc. 38 (1916) 2221–2295.

[42] K.R. Hall, L.C. Eagleton, A. Acrivos, T. Vermeulen, Pore-and solid-diffusion kinetics in fixed-bed adsorption under constant-pattern conditions, Ind. Eng. Chem. Fundam. 5 (1966) 212–223.

[43] H. Freundlich, Über die adsorption in lösungen Zeitschrift für physikalische, Chemie 57 (1907) 385–470.

[44] M. Temkin, Kinetics of ammonia synthesis on promoted iron catalysts Acta physiochim, URSS 12 (1940) 327–356.

[45] A. Hashem, H. A. Hammad and A. Al-Anwar, Chemically modified Retama raetam biomass as a new adsorbent for Pb(II) ions from aqueous solution: non-linear regression, kinetics and thermodynamics, Green Process Synth. 4 (2015) 463–478.

[46] H. Jiang, Y. Zhang, R. Chen, M. Sun, H. Tong, J. Xu, Preparation of ion imprinted magnetic Fe3O4 nanoparticles for selective remediation of Pb(II). J Taiwan Inst Chem. Eng. 80 (2017) 184–191.

[47] M.N.M. Ibrahim, W.S. W. Ngah, M.S. Norliyana, W.R. W. Daud, M. Rafatullah, O. Sulaiman, R. Hashim, A novel agricultural waste adsorbent for the removal of lead (II) ions from aqueous solutions, J. Hazard. Mater. 182 (2010) 377–385.

[48] Q. Xu, Y. Wang, L. Jin, Y. Wang, M. Qin, Adsorption of Cu (II), Pb (II) and Cr (VI) from aqueous solutions using black wattle tannin-immobilized nanocellulose, J. Hazard. Mater. 339 (2017) 91–99.

[49] N. Azouaou, Z. Sadaoui, A. Djaafri, H. Mokaddem, Adsorption of cadmium from aqueous solution onto untreated coffee grounds: Equilibrium, kinetics and thermodynamics, J. Hazard. Mater. 184 (2010) 126–134.

[50] W. Chen, Z. Lu, B. Xiao, P. Gu, W. Yao, J. Xing, A.M. Asiri, K.A. Alamry, X. Wang, S. Wang, Enhanced removal of lead ions from aqueous solution by iron oxide nanomaterials with cobalt and nickel doping, J. Clean. Prod. 211 (2019) 1250–1258.

[51] R.P. Mohubedu, P.N.E. Diagboya, C.Y. Abasi, E.D. Dikio, F. Mtunzi, Magnetic valorization of biomass and biochar of a typical plant nuisance for toxic metals contaminated water treatment, J. Clean. Prod. 209 (2019) 1016–1024.

[52] S.K. Lagergren About the theory of so-called adsorption of soluble substances. Sven Vetensk Handingarl 24(1898)1–39.

[53] Y-S. Ho, G. McKay, Pseudo-second order model for sorption processes. Process Biochem 34(1999) 451–465.

[54] W.J. Weber, J. C. Morris (1963) Kinetics of adsorption on carbon from solution. J. Sanit. Eng. Div. 89 (1963) 31–60.

[55] F. Marrakchi, M. Ahmed, W. Khanday, M. Asif, B. Hameed, Mesoporous-activated carbon prepared from chitosan flakes via single-step sodium hydroxide activation for the adsorption of methylene blue. Int J Biol Macromol 98(2017)233–239.

[56] D. Kołodyńska, P. Hałas, M. Franus, Z. Hubicki, Zeolite properties improvement by chitosan modification—sorption studies. J. Ind. Eng. Chem. 52(2017) 187–196.

[57] E. Tutem, R. Apak, C.F. Unal, Adsorptive removal of chlorophenols from water by bituminous shale, Water Res. 32 (1998) 2315–2324.

[58] L.R. Somera, R. Cuazon, J. K. Cruz, L.J. Diaz, Kinetics and isotherms studies of the adsorption of H (II) onto iron modified montmorillonite/polycaprolactone nanofiber membrane. In: IOP Conference Series: materials science and engineering, IOP Publishing, 540(2019) p 012005.

[59] V.K. Gupta, Equilibrium uptake, sorption dynamics, process development and column operations for the removal of copper and nickel from aqueous solution and wastewater using activated slag: A low-cost adsorbent, Ind. Eng. Chem. Res. 37 (1998) 192–202.

518 **Tables**

519

520 **Table 1:** List of non-linear error functions used in this study

Error Function	Equation	References
Average Relative Error (ARE)	$ARE = \sum_{i=1}^{n} \left\| \frac{(q_e)_{\text{exp.}} - (q_e)_{calc.}}{(q_e)_{\text{exp.}}} \right\|$	24
Average Percentage Error (APE)	$APE\% = \frac{\sum_{i=1}^{N} \left\| [((q_e)_{\text{exp.}} - (q_e)_{calc.}) / q_{\text{exp.}}] \right\|}{N} x100$	25
Sum Squares Error (ERRSQ/SSE)	$ERRSQ = \sum_{i=1}^{n} [(q_e)_{calc.} - (q_e)_{\text{exp.}}]^2$	26
Hybrid Fraction Error Function (Hybrid)	$Hybrid = \frac{100}{n-p} \sum_{i=1}^{n} [\frac{((q_e)_{\text{exp.}} - (q_e)calc.)^2}{(q_e)_{\text{exp.}}}]_i$	27
Marquardt's Percent Standard Deviation MPSD	$MPSD = (\sqrt{\frac{1}{n-p} \sum_{i=1}^{n} [\frac{((q_e)_{\text{exp.}} - (q_e)_{calc.})}{(q_e)_{\text{exp.}}}]^2}$	28
Sum of Absolute Error (EABS)	$EABS = \sum_{i=1}^{n} \left\| (q_e)_{\text{exp.}} - (q_e)_{calc.} \right\|_i$	29
Nonlinear chi-square test(χ^2)	$\chi^2 = \sum \frac{(q_{e.\text{exp}} - q_{e.theoretical})^2}{q_{e.theoretical}}$	30
Coefficient of determination (R^2)	$R^2 = \frac{\sum_{i=1}^{n} (q_{e,calc} - \overline{q_{e,\text{exp}}})^2}{\sum_{i=1}^{n} (q_{e,calc} - \overline{q_{e,\text{exp}}})^2 + \sum_{i=1}^{n} (q_{e,calc} - q_{e,\text{exp}})^2}$	31

521

522 **Table 2**: Comparison of adsorption capacities of various adsorbents for Pb(II)

Adsorbent	Adsorption Capacity(mg/g)	References
Modified Ratama raetam	270.27	1
Magnetic polymer (Pb-IIMP)	123.3	2
Carpobrotus edulis	175.6	3
Tannin-nanocellulose (TNCC)	53.37	4
Coffee residue activated with zinc chloride	62.57	5
$NiFe_2O_3$	97.5	6
Biomass-magnetic hybrid	63.6	7
Modified microcrystalline cellulose(MMCC)	1155	Present study

523

Table 3: Isotherm constants of two-parameter models for Pb(II) ions adsorption onto MMCC at 30 °C

Isotherm Model	Parameter	Value	Error Analysis	Value
Langmuir	a_L	0.0055 L/mg	ARE	0.4018
	q_{max}	1155.04 mg/g	APE%	5.022
	k_L	6.30 L/g	EABS	280.0
	R_L	0.578	ERRSQ	16267
			R^2	0.9965
Freundlich	n	2.69	ARE	0.3970
	K_F	85.80 mg/g	APE%	4.962
			EABS	207.9
			ERRSQ	15351
			R^2	0.9969
Tempkin	A_T	0.0816 L/g	ARE	0.5567
	b_T	11.23 mg/L	APE%	6.959
			EABS	354.9
			ERRSQ	28622
			R^2	0.9937

Table 4: Kinetic parameters for the adsorption of Pb(II) ions onto MMCC at 303 mg/L and 493 mg/L.

Parameters	C_o(mg/L)	
	303	493
Pseudo-first-order		
q_e(mg/g)	640.8	640.8
K_1(1/min)	0.0359	0.0359
ARE	1.395	0.8556
APE %	12.68	7.780
EABS	468.5	467.5
ERRSQ	32454	29985
Hybrid	111.11	60.02
MPSD	0.4210	0.1355
χ^2	186.66	73.16
R^2	0.9946	0.9933
Pseudo-second-order		
q_e(mg/g)	727.8	813.5
K_2(g/mg.min)	5.93961E-05	0.000125472
ARE	0.9007	0.3651
APE %	8.188	3.319
EABS	278.6	175.5
ERRSQ	13996	6059.8
Hybrid	54.58	15.52
MPSD	0.2251	0.0421
χ^2	84.35	18.63
R^2	0.9987	0.9986
Intra-Particle		
k id	0.99999	1.0000
C	5.01807E-05	1.03015E-07
ARE	10.83	10.87
APE %	98.47	98.86
EABS	4956	6713
ERRSQ	2477462	4322597
Hybrid	4874.15	6631.41
MPSD	10.67	10.75
χ^2	312000	606539
R^2	0.0777	0.0808
Bangham Model		
q_e(mg/g)	775.7	813.5
k_b	0.1367	0.2421
n	0.4993	0.5032
ARE	0.2716	0.1473
APE %	2.4689	1.3394
EABS	112.7	79.0
ERRSQ	2409.1	1129.4
Hybrid	5.61	2.39
MPSD	0.0157	0.0053
χ^2	5.65	2.28
R^2	0.9991	0.9997

Table 5: Thermodynamic parameters of Pb(II) ions onto MMCC at different temperatures

Temperature (°C)	ΔG^o (kJ.mol^{-1})	ΔH^o (kJ.mol^{-1})	ΔS^o (JK^{-1}.mol^{-1})
30	12.373	49.141	112.77
50	13.128		
60	13.967		

Figures

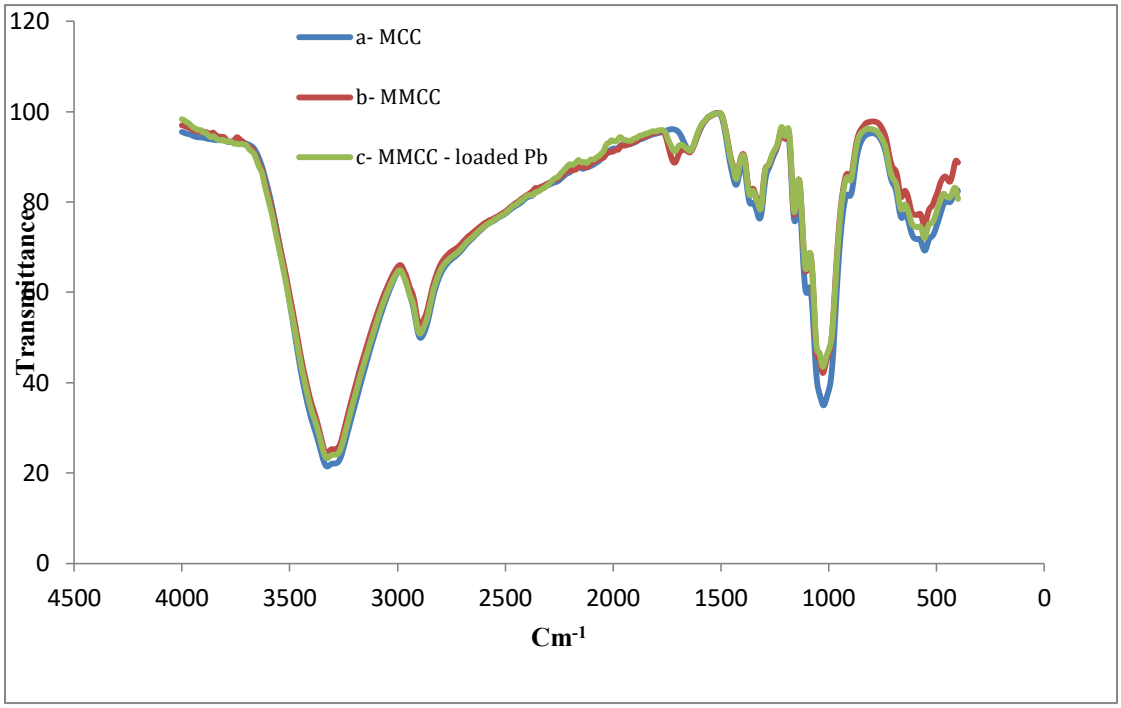

Figure 1: FT-IR spectra of (a) MCC; (b) MMCC; (c) MMCC-loaded Pb(II) ions.

554 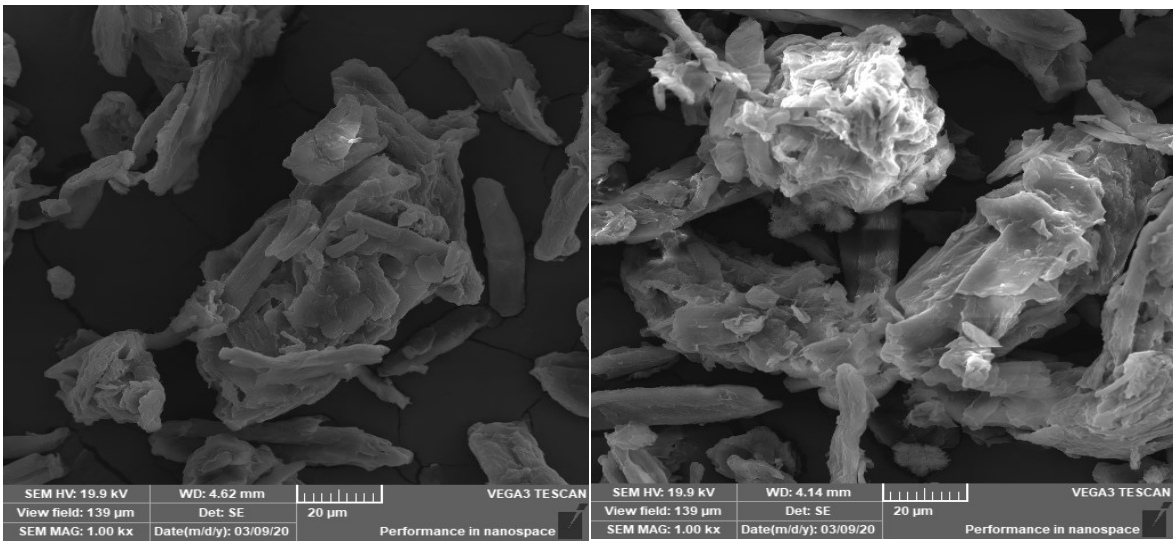

555 **(a)** **(b)**

556 

557 **(c)**

558 **Figure 2:** SEM images of (a) MMCC;(b) MMCC loaded -Pb(II) ions; (c) associated energy-dispersive X-ray
559 analysis (EDX) patterns for MMCC and MMCC loaded -Pb(II) ions.

560

561

562

563

564

565

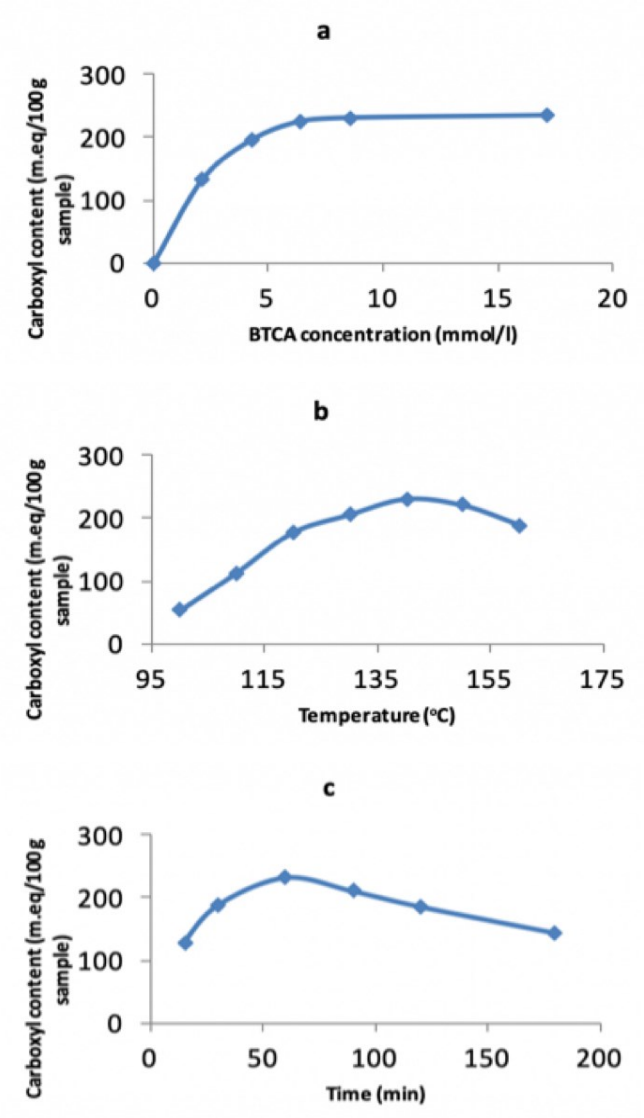

566

567

568 **Figure 3:** Effect of different factors: (a) BTCA concentration; (b) reaction temperature and (c) reaction time
569 on the extent of modification of MMCC.

570 Reaction conditions: (a) MCC conc. 12.34 mmol/L; reaction temperature 140 °C; reaction time 1 h; (b)
571 MCC conc. 12.34 mmol/L; BTCA, 8.547 mmol/L; reaction time 1 h; (c) MCC conc. 12.34 mmol/L; BTCA,
572 8.547 mmol/L reaction temperature 140 °C.

573

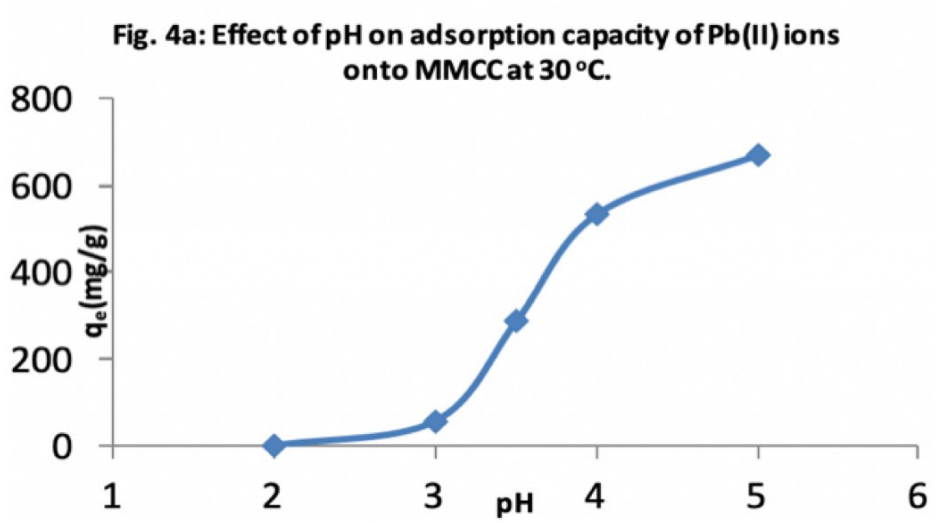

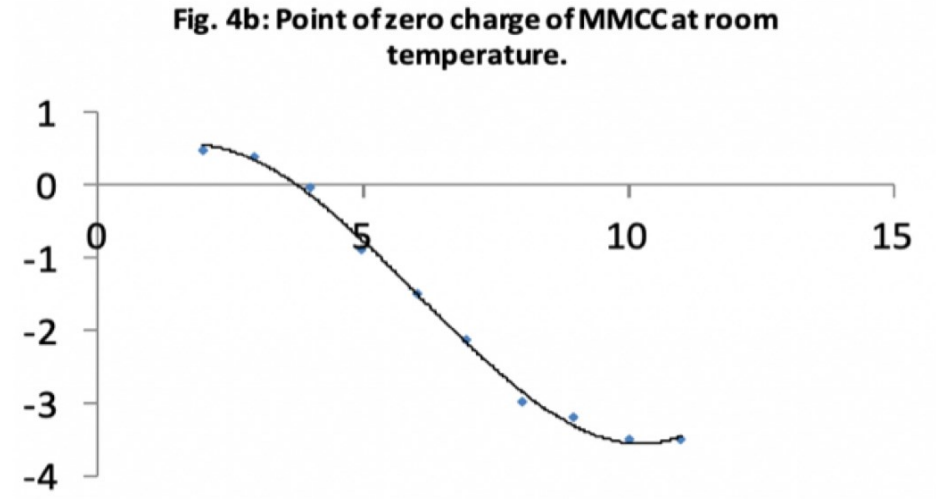

574

575

576 **Figure 4:** (a) Effect of pH on adsorption capacity of Pb(II) ions onto MMCC at 30 °C.

577 Reaction Conditions: Pb(II) conc. 400 mg/L; MMCC conc. 0.3g/L; contact time 3 h; reaction temperature
578 30 °C; COOH content 231 m.eq/100 g sample; (b) Point of zero charge of MMCC.

579

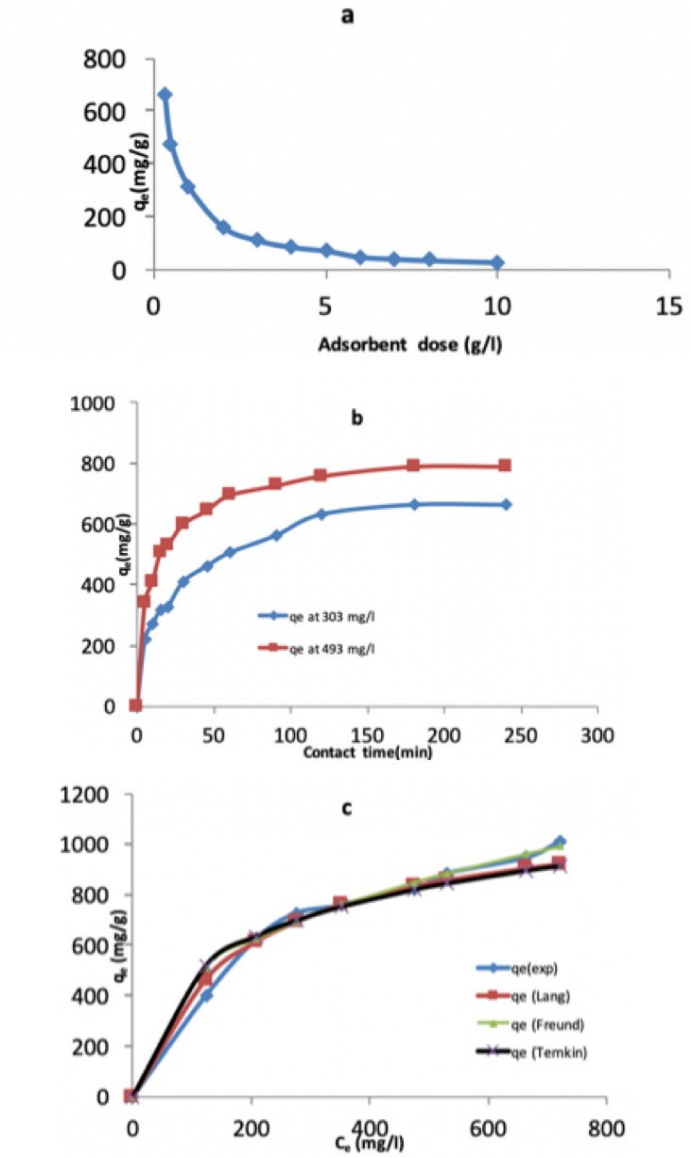

580

581

582 **Figure 5:** Effect of different variables: (a) adsorbent concentration; (b) contact time and (C) adsorbate
583 concentrations on adsorption capacity of Pb(II) ions onto MMCC at 30 °C.

584 Reaction Conditions: (a) Pb(II) conc. 400 mg/L; pH 5; contact time 3 h; reaction temperature 30 °C;
585 COOH content 231 m.eq/100 g sample; (b) Pb(II) conc. 400 mg/L; MMCC conc. 0.3 g/L; pH 5; reaction
586 temperature 30 °C; COOH content 231 m.eq/100 g sample; (c) MMCC conc. 0.3 g/L; pH 5; contact time 3
587 h; reaction temperature, 30 °C; COOH content 231 m.eq/100 g sample.

588

589

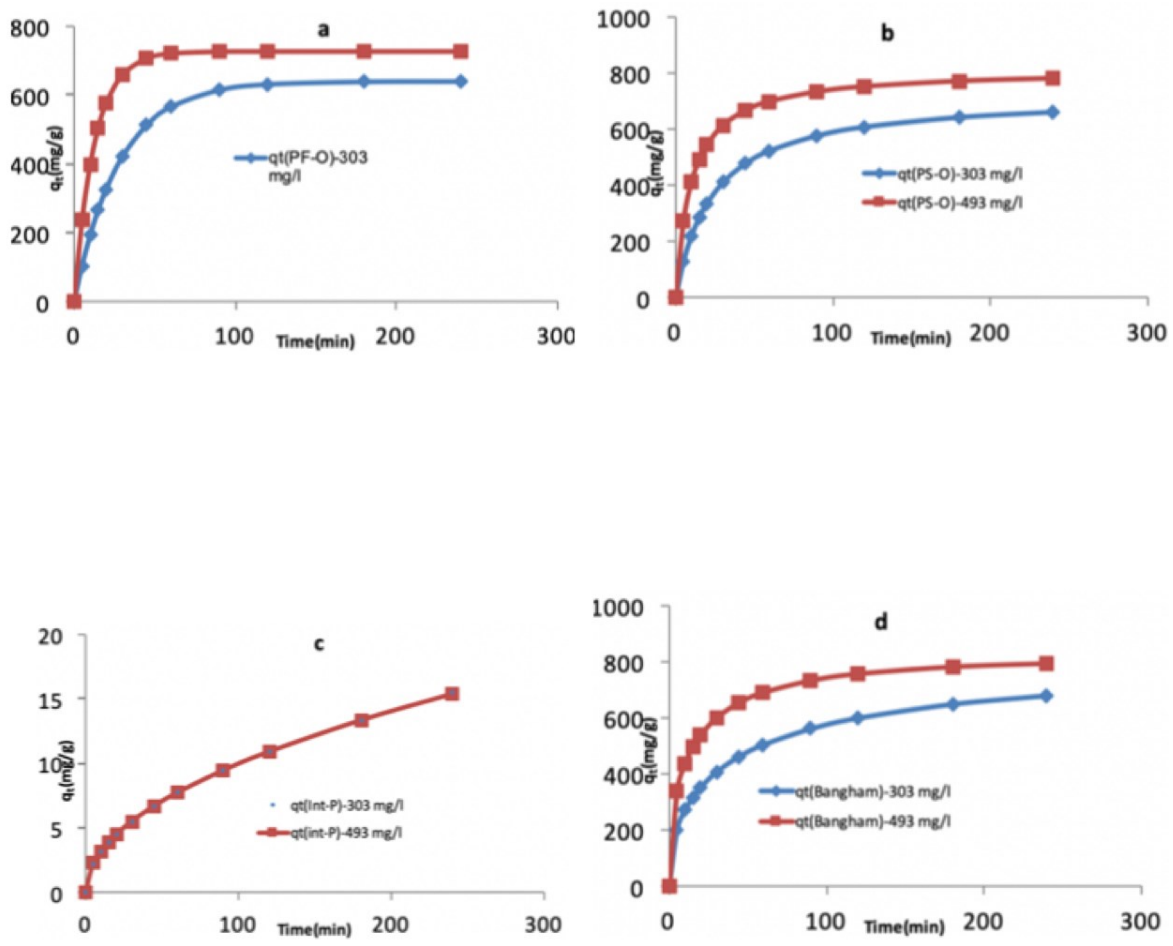

590

591 **Figure 6:** Non-linear plots of (a) pseudo first-order; (b) pseudo second order; (c) intra-particle diffusion
592 and (d) Bangham models for adsorption of Pb(II) ions onto MMCC (micocrystalline cellulose (MMC)
593 modified with 1, 2, 3, 4-butanetetracarboxylic acid (BTCA)) at 303 mg/L and 493 mg/L.

594 Reaction Conditions: Pb(II) conc. 400 mg/L; MMCC conc. 0.3 g/L; pH 5; reaction temperature 30 °C;
595 COOH content 231 m.eq/100 g sample

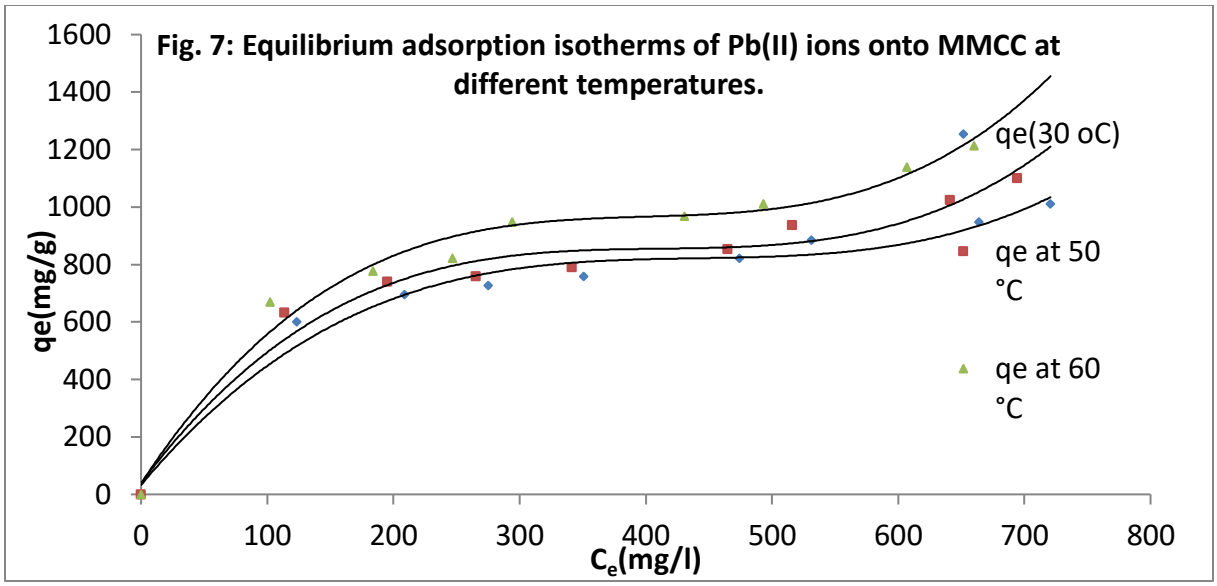

596

597 **Figure 7:** Equilibrium adsorption isotherms of Pb(II) ions onto MMCC (micocrystalline cellulose (MMC)
598 modified with 1, 2, 3, 4-butanetetracarboxylic acid (BTCA))at 30, 50 and 60 °C. Reaction Conditions:
599 MMCC conc. 0.3 g/L; pH 5; contact time 3 h; COOH content 231 m.eq/100 g sample.

600

601